Journal of Magnetic Resonance 324 (2021) 106913

Contents lists available at ScienceDirect

Journal of Magnetic Resonance

journal homepage: www.elsevier.com/locate/jmr

Isotropic solid-state MQMAS NMR spectra for large quadrupolar interactions using satellite-transition selective inversion pulses and low rf fields

Ivan Hung *, Zhehong Gan

National High Magnetic Field Laboratory, 1800 East Paul Dirac Drive, Tallahassee, FL 32310, USA

ARTICLE INFO

Article history:
Received 9 December 2020
Revised 4 January 2021
Accepted 12 January 2021
Available online 21 January 2021

Keywords:
High-resolution
Quadrupolar nuclei
Solid-state NMR
Multiple quantum magic angle spinning
MQMAS
Large quadrupolar interactions

ABSTRACT

Multiple-quantum magic-angle spinning (MQMAS) pulse sequences are presented that are capable of obtaining isotropic NMR spectra for large quadrupolar interactions using lower rf fields. These experiments rely on rotor period long pulses applied at a large offset from the central-transition, making them selective to the satellite-transitions. Each such pulse gives rise to an anisotropic phase, which can be cancelled to obtain coherent signal evolution if a pair of pulses are applied in a symmetric manner. Thus, efficient excitation and conversion of triple-quantum coherences from and to the central-transition is achieved for MQMAS even for large quadrupolar couplings, by selective inversion of the satellite-transitions using such low-power pulses. Low-power multiple-quantum magic-angle spinning (lpMQMAS) pulse sequences are demonstrated on a model compound, $RbNO_3$, and also applied on β-Ga_2O_3, a sample with the largest quadrupolar interactions for which isotropic NMR spectra have been obtained to date.

1. Introduction

Resolution of distinct atomic sites is a defining feature of NMR spectroscopy. In the absence of isotropic motion, anisotropic interactions usually lead to broadening of NMR resonances and loss of resolution for non-liquid samples. For nuclei with spin quantum numbers $S = 1/2$, magic-angle spinning (MAS) of the sample can regain isotropic spectral resolution. However, for nuclei with $S > 1/2$, which make up most of the NMR-active nuclei in the Periodic Table, MAS alone is insufficient due to the presence of the high-rank second-order quadrupolar broadening. Isotropic resolution can be obtained for half-integer quadrupolar nuclei (S = 3/2, 5/2, 7/2, 9/2) by spinning the sample at two different angles with respect to the external magnetic field B_0 either simultaneously or sequentially, as in the double rotation (DOR) [1] or dynamic angle spinning (DAS) techniques [2], respectively. Both these methods require specialized equipment and have thus not seen widespread application. As an alternative, experiments such as multiple-quantum magic-angle spinning (MQMAS) [3], and satellite-transition magic-angle spinning (STMAS) [4] have been developed, which only require conventional MAS probes; facilitating their widespread use, in particular the more robust MQMAS method.

The MQMAS and STMAS experiments require high radiofrequency (rf) fields to refocus the second-order quadrupolar interaction. However, as the magnitude of the quadrupolar interaction increases, rf fields high enough for efficient manipulation of the multiple-quantum (MQ) and satellite-transition (ST) coherences for MQMAS and STMAS, respectively, can no longer be practically achieved. These 2D experiments are thus met with a rather hard limit in the maximum quadrupolar couplings (C_Qs) to which they can be successfully applied. To our knowledge, application of MQMAS and STMAS have not been reported for any half-integer nuclei with quadrupolar frequencies $\nu_Q = 3C_Q/[2S(2S-1)]$ above 2.5 MHz.

Recently, the authors have demonstrated that such a limitation can be lifted for the STMAS experiment by using 'long' pulses of a rotor period τ_r in duration (henceforth, simply denoted as τ_r-pulses). The τ_r-pulses are applied far off-resonance from the central-transition (CT) for excitation and conversion of the STs in a manner which is relatively insensitive to the magnitude of C_Q [5]. However, STMAS requires stringent experimental conditions to properly average the first-order quadrupolar interaction of the STs, such as a very accurate magic-angle setting, and MAS speed stability [6]. Therefore, there is motivation to explore the applicability of τ_r-pulses in MQMAS experiments, for which such strict experimental conditions are not necessary. As such, MQMAS sees

* Corresponding author.
E-mail address: hung@magnet.fsu.edu (I. Hung).

https://doi.org/10.1016/j.jmr.2021.106913
1090-7807/

much broader application though it sits at a disadvantage in terms of sensitivity compared to STMAS [7].

In essence, the present work extends the application of τ_r-pulses, previously used to excite the innermost STs in the low-power STMAS experiment [5], to serve instead as ST π-pulses in MQMAS experiments. In principle, an ideal inversion of the |±1/2> and |±3/2> spin states would achieve full interconversion between the CT single-quantum (1Q) and triple-quantum (3Q) coherences, yielding a very efficient way of performing MQMAS. Emphatically, τ_r-pulses need to be applied in pairs, with changes in coherence that are of equal order but opposite in sign, to avoid destructive interference between the distributions in phase encoding generated by each individual τ_r-pulse [5,8]. MQMAS pulse sequences using such principles are presented that can give isotropic spectra for much larger quadrupolar interactions than previously possible using low rf power.

2. Theory

For a rotating sample with large anisotropic interactions under MAS, the instantaneous frequency of each crystallite sweeps across the powder pattern during a rotor cycle. Therefore, application of a rotor-period (τ_r) long pulse allows all crystallites to eventually encounter the frequency of rf irradiation at some point during τ_r. For half-integer quadrupolar nuclei, this picture is complicated by the CT, which is unaffected by the first-order quadrupolar interaction. However, a simplification can be made by placing the rf irradiation frequency ν_{irr} far from the CT, while remaining within the STs. Then, taking S = 3/2 nuclei as an example, the two STs can be treated as two independent two-level systems, and an average rf spin Hamiltonian can be derived in a jolting frame [8–11] (i.e., the interaction frame of the quadrupolar interaction modulated by MAS),

$$\bar{h}/2\pi = \Delta\bar{\nu}_n I_z + \nu_1\sqrt{3}|s_n|e^{-i\varphi I_z}I_x e^{i\varphi I_z} \quad (1)$$

where $\Delta\bar{\nu}_n$ is the frequency offset of the nth spinning sideband nearest to ν_{irr}, $[I_x, I_y, I_z]$ are fictitious S = 1/2 operators for the two-level sub-systems, and ν_1 is the amplitude of the rf field. The second term on the right of Eq. (1) is the rf Hamiltonian scaled by the intensity of the nth ST ssb of an individual crystallite

$$|s_n| \sim \sqrt{\nu_r/(1.5\nu_Q)} < 1 \quad (2)$$

where ν_r (= $1/\tau_r$) is the sample spinning frequency, the quadrupolar frequency ν_Q is equal to $3C_Q/[2S(2S-1)]$, and $1.5\nu_Q$ is the breadth of one ST without considering the asymmetry parameter η_Q. The estimate in Eq. (2) is obtained from the normalized ssb intensities, i.e. $\sum_n|s_n|^2 = 1$, and an assumption that all ssbs have equal intensities. Therefore, an effective rf field for τ_r-pulses of $\nu_1^{eff} \sim \nu_1\sqrt{3}|s_n| = \nu_1\sqrt{2\nu_r/\nu_Q}$ is obtained, which can excite the STs efficiently; noting particularly that the large first-order quadrupolar offset becomes absent in the jolting frame. In addition, Eq. (1) shows that the rf phase experienced by each crystallite is shifted by the phase ϕ of the complex intensity for the nth ssb nearest to ν_{irr}. Hence, application of τ_r-pulses to a powder sample yields only slightly coherent magnetization because of the rf phase variation amongst crystallites, i.e., the signal phase is anisotropic. It is then crucial to apply τ_r-pulses in pairs to induce changes in coherence order that are symmetric (i.e., of equal magnitude but opposite signs) and cancel the phase incoherence generated by each individual pulse [8,12].

For low-power STMAS [5], the aim was to achieve maximum excitation of the STs (Δp = ±1) using τ_r-pulses (i.e., $\nu_1^{eff}\tau_r = 1/4$), which theoretically requires an rf field of $\nu_1 \sim \sqrt{\nu_Q\nu_r/32}$. For 'low-power' MQMAS, selective inversion of the STs (Δp = ±2) is necessary to interconvert between CT and 3Q coherences, therefore the optimal rf field should in theory be doubled, i.e., $\nu_1 \sim \sqrt{\nu_Q\nu_r/8}$. The weak dependence of the optimal ν_1 on ν_Q is of key importance for the applicability of τ_r-pulses to nuclei with large quadrupolar interactions.

3. Pulse sequence design

One of the simplest implementations of the MQMAS experiment is the three-pulse z-filter pulse sequence (Fig. 1a) [13]. To date, the most effective and robust method of exciting 3Q transitions is the application of a short, high-power pulse (Fig. 1a, orange pulse) starting from 3Q polarization, as depicted by the coherence transfer pathway in the density matrix diagram in Fig. 1b. The magnitude of quadrupole couplings accessible by such an approach have been shown by experiments and simulations to be limited [5,14]. To our knowledge, there has not been an application of MQMAS experiments to nuclei with quadrupolar frequencies ν_Q > ~2.5 MHz. Thus, an alternative approach is necessary to allow application of MQMAS to larger quadrupolar interactions.

If instead of exciting 3Q polarization, CT 1Q coherence is first excited with a CT-selective π/2-pulse (Fig. 1c, first red pulse), a ST π τ_r-pulse (Fig. 1c, first blue pulse) would invert the |±1/2> ↔ |±3/2> states and interconvert CT 1Q and 3Q coherences, as depicted by the coherence transfer pathway in the density matrix diagram of Fig. 1d. Such an interconversion is reminiscent of using CT-selective π-pulses for interconversion of 1Q and 2Q ST coherences in the double-quantum filtered STMAS experiment [15]. Thus, the two short, high-power pulses in the conventional pulse sequence (Fig. 1a, orange and purple pulses) are replaced by what can be considered 'composite' pulses, each consisting of an on-resonance CT-selective π/2-pulse concatenated with an off-resonance 'ST-selective' inversion τ_r-pulse (Fig. 1c), that break up each 0Q ↔ 3Q process into two sequential steps transiting through CT 1Q coherence. MQMAS experiments with such 'composite' pulses will henceforth be denoted as 'low-power' MQMAS, or lpMQMAS, since they require much lower rf fields/power compared to conventional sequences, as demonstrated experimentally below. It is emphasized that the irradiation frequency ν_{irr} for τ_r-pulses should be far off-resonance from the CT, while remaining within the ST manifold.

As an alternative to using a z-filter, τ_r-pulses can also be used in phase-modulated shifted-echo lpMQMAS pulse sequences with or without split-t_1 acquisition [16,17], as shown in Fig. 1f, in analogy to sequences using short, hard pulses for 3Q excitation and conversion (Fig. 1e). As has been discussed in the literature [16,17], shifted-echo sequences select one of two MQ coherence transfer pathways corresponding to the echo which travels forward in time as t_1 is increased. Absorptively phased spectra can be obtained when whole echo signals are acquired along the t_2 dimension. For the acquisition of shifted-echo lpMQMAS spectra of S = 3/2 nuclei without split-t_1 acquisition (i.e., k' = k'' = 0), the hashed π-pulse needs to be applied while selecting the coherence transfer pathway drawn as a solid line in Fig. 1f. For all other cases, the coherence transfer pathway drawn as a dashed line is chosen, and the hashed π-pulse is omitted. The k values used for split-t_1 acquisition are the ratios between the second-order quadrupolar broadenings of the 3Q and CT transitions for S = 3/2 (k') and S > 3/2 (k'') nuclei, respectively. It is worth noting that the shifted-echo pulse sequence in Fig. 1f bears some resemblance to the rotation-induced adiabatic coherence transfer (RIACT) method for MQMAS [18]. However, the underlying theory and principles used to design the RIACT and lpMQMAS experiments are different, leading most importantly to a large difference in the irradiation frequency and duration of the long pulses used in the two

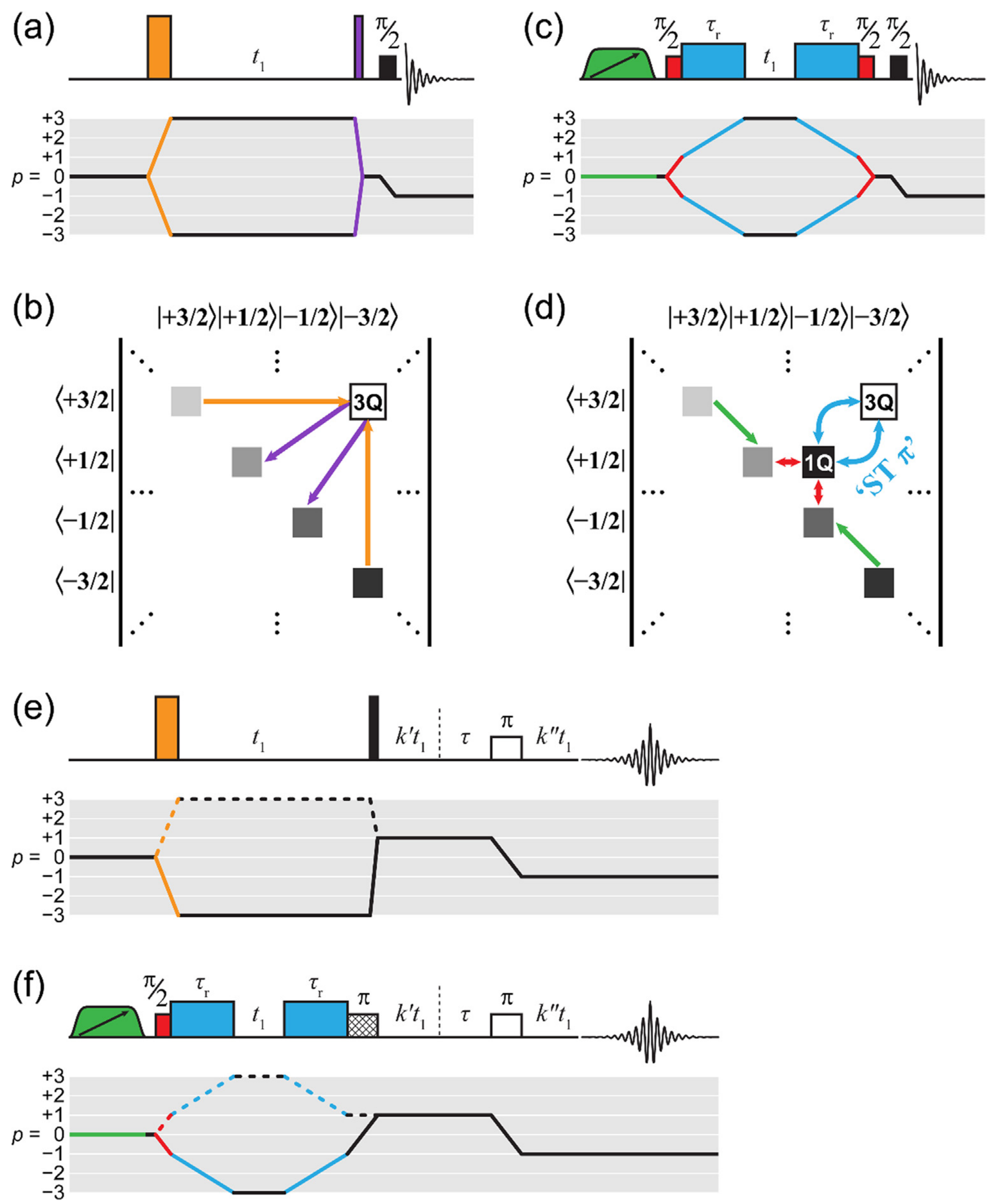

Fig. 1. Pulse sequence schematics and coherence transfer pathway diagrams for the (a) conventional three-pulse z-filter MQMAS, (c) z-filter lpMQMAS, (e) conventional shifted-echo MQMAS, and (f) shifted-echo lpMQMAS experiments. Density matrix diagrams illustrating the action of color-coded pulses for the (b) conventional three-pulse z-filter MQMAS pulse sequence, and the (d) z-filter lpMQMAS pulse sequence; pulse actions are symmetric about the diagonal, so only actions above the diagonal are shown. The τ_r-pulses shown in blue are of particular importance in this work and are applied far off-resonance from the CT to selectively invert the STs. Ideal ST π-pulses would interconvert between CT 1Q and 3Q coherences. Frequency-swept WURST pulses (shown in green) can be used to enhance the sensitivity of lpMQMAS experiments. The pulse sequences in (e) and (f) can be used to acquire split-t_1 experiments by selecting the coherence pathways shown as dashed lines, where $k' = (7/9, 0, 0, 0)$ and $k'' = (0, 19/12, 101/45, 91/36)$ for $S = (3/2, 5/2, 7/2, 9/2)$. The hashed π-pulse in (f) is only applied for shifted-echo lpMQMAS experiments of $S = 3/2$ nuclei without split-t_1 ($k' = k'' = 0$) acquisition, otherwise it should be omitted. The coherence transfer pathways drawn as solid lines in (e) and (f) are selected only for shifted-echo experiments on $S = 3/2$ nuclei without split-t_1 acquisition, otherwise the dashed pathway should be selected. For convenience, the basic shifted-echo lpMQMAS pulse sequence in Bruker format is included in the Appendix. (For interpretation of the references to color in this figure legend, the reader is referred to the web version of this article.)

methods. The off-resonance ST-selective inversion pulses used for lpMQMAS make it more efficient, and also capable of accessing greater quadrupolar interactions.

Note that lpMQMAS experiments begin from equilibrium CT magnetization, therefore it is possible to enhance their sensitivity by inversion/saturation of the STs using methods such as rotor-assisted population transfer (RAPT) [19], double frequency sweep (DFS) [20], hyperbolic secant (HS) pulses [21], or quadruple frequency sweep (QFS) [22] prior to application of the initial CT-selective $\pi/2$-pulse. In principle, these signal enhancement methods should always be applied in lpMQMAS experiments as their only disadvantage would be the absence of any effect, but the potential signal increase can reach up to two times the spin quantum number 2*S*. For simplicity, off-resonance, frequency-swept, wideband, uniform rate, smooth truncation (WURST) [23] pulses are used for signal enhancement [24] in the present work, as denoted by the green, shaped pulses in Fig. 1c and f.

4. Experimental results

As a proof of principle, lpMQMAS experiments are first applied on a compound with modest quadrupole coupling constants ($C_Q \sim 1.9$ MHz) [25]. The signal intensity of the conventional shifted-echo MQMAS experiment (black trace) and the shifted-echo lpMQMAS experiment (orange trace) are compared with a spin-echo spectrum (blue trace) for the ^{87}Rb (S = 3/2) nuclei of $RbNO_3$ in Fig. 2a. The integrated intensity of the lpMQMAS spectrum (0.15) is approximately half compared to that of the MQMAS spectrum (0.28). Notably, the short, hard pulses used for MQMAS were applied with ν_1 = 115 kHz, whereas the τ_r-pulses in lpMQMAS only required a power level equivalent to an on-resonance rf field of ν_1 = 24 kHz. The lower rf field requirement for lpMQMAS compared to MQMAS is important for applications to low-γ nuclei, for which high ν_1 are inherently difficult to obtain. The lpMQMAS signal of 0.15 also indicates that each of the τ_r-pulses has a ST inversion efficiency of approximately $\sqrt{0.15} \approx 0.4$. This is remarkably high given the large difference in magnitude between the applied ν_1 of a few tens of kilohertz and the breadth of the STs, which is on the order of a few megahertz. The ability of τ_r-pulses to efficiently excite and invert STs stems from the modulation of the anisotropic frequency of each crystallite by MAS, which allows each crystallite to come into resonance with the rf irradiation at some point during the rotor period. Symmetric pair-wise application of the τ_r-pulses cancels the anisotropic rf phase distribution. Thus, the distribution in magnitude of the effective rf field becomes the main factor leading to non-ideal ST inversion.

Polarization enhancement can be added to lpMQMAS experiments, which excite MQ coherence from CT coherence. Application of a 1 ms WURST pulse at ν_{irr} = +220 kHz before lpMQMAS results in a signal intensity of 0.36; an improvement over conventional MQMAS of ~30%. The signal enhancement of 0.36/0.15 = 2.4 from ST saturation/inversion is consistent with the enhancement observed on 1D spin-echo spectra (not shown). Such polarization enhancement is not applicable to conventional MQMAS experiments that excite 3Q polarization directly. Notably, the amount of signal enhancement from ST saturation/inversion techniques can vary among different samples. The above comparison shows that lpMQMAS can outperform conventional MQMAS experiments for samples with moderate C_Q values using low rf fields.

The ^{87}Rb 2D shifted-echo lpMQMAS NMR spectrum of $RbNO_3$, after shearing the f_1 dimension into an isotropic representation, is shown in Fig. 2b. Similar spectra (not shown) were obtained with split-t_1 acquisition by selecting the coherence transfer pathway drawn as a dashed line in Fig. 1f and setting k' =7/9 and k'' = 0, as well as using the z-filter experiment in Fig. 1c. Demonstrating that τ_r-pulses are generally applicable in different types of MQMAS experiments without causing artifacts.

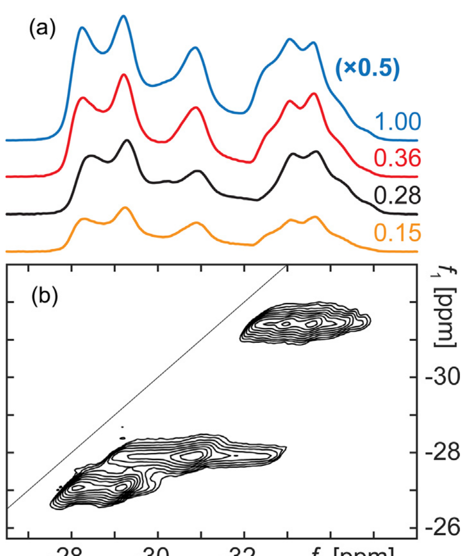

Fig. 2. (a) Comparison of ^{87}Rb (S = 3/2) NMR signal intensities of the WURST-enhanced shifted-echo lpMQMAS (red), conventional shifted-echo MQMAS (black), and shifted-echo lpMQMAS (orange) experiments for $RbNO_3$. The signal intensities are normalized with respect to a spin-echo spectrum (blue), which has been scaled down vertically by a factor of two to ease visual comparison. (b) ^{87}Rb 2D shifted-echo lpMQMAS NMR spectrum of $RbNO_3$ sheared into an isotropic f_1 representation. The base contour level is set at 3% of the maximum intensity. Spectra were acquired at 19.6 T with a Bruker Avance NEO console, ν_r = 10 kHz MAS, recycle delay of 0.15 s, CT-selective π/2- and π-pulses of 20 and 40 μs at ν_1 = 6.25 kHz, and full-echo acquisition with a half-echo delay of 1 ms. For MQMAS, 3Q excitation and conversion pulses of 5.2 and 1.75 μs with ν_1 = 115 kHz were used, while τ_r-pulses with ν_1 = 24 kHz were used for lpMQMAS at ν_{irr} = +22ν_r = +220 kHz. When applied, signal enhancement for lpMQMAS spectra was performed using a 1 ms WURST-80 pulse with a sweep range equal to ν_r, ν_1 = 12 kHz, and ν_{irr} = +220 kHz. The 2D shifted-echo lpMQMAS spectrum was acquired with WURST enhancement, 64 rotor-synchronized t_1 increments, and 96 transients per increment, resulting in a total experiment time of 22 minutes. (For interpretation of the references to color in this figure legend, the reader is referred to the web version of this article.)

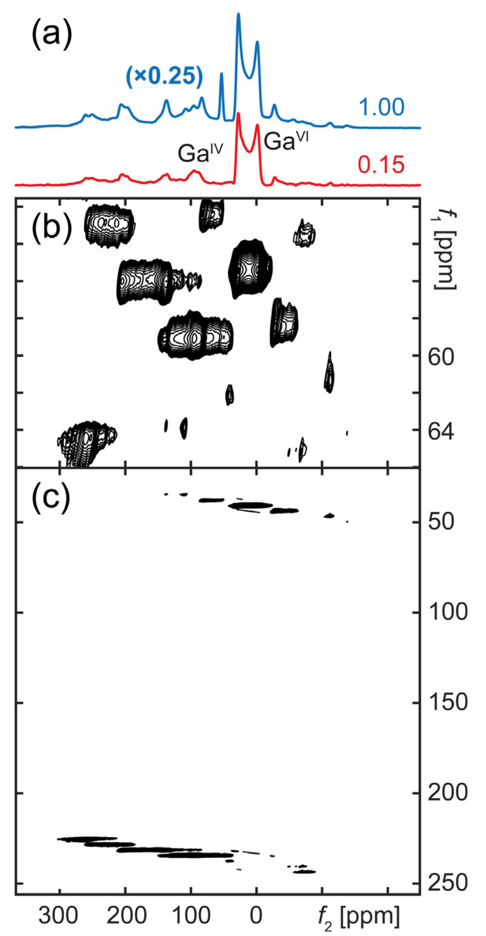

Fig. 3. (a) Comparison of the ^{71}Ga (S = 3/2) NMR signal intensity of the WURST-enhanced shifted-echo lpMQMAS (red) experiment for β-Ga_2O_3 and a spin-echo spectrum (blue). The signal intensities are normalized with respect to a spin-echo spectrum (blue), which has been scaled down vertically by a factor of four to ease visual comparison. (b) ^{71}Ga 2D shifted-echo lpMQMAS NMR spectrum of β-Ga_2O_3 sheared into an isotropic f_1 representation. (c) ^{71}Ga 2D shifted-echo lpMQMAS NMR spectrum after Q-shearing, expansion of the f_1 spectral width and shearing into an isotropic f_1 representation to unravel spectral folding. The base contour levels are set at 3% of the maximum intensity. Spectra were acquired at 19.6 T with a Bruker Avance NEO console, ν_r = 14 kHz MAS, recycle delay of 3.5 s, CT-selective π/2- and π-pulses of 2.5 and 5.0 μs at ν_1 = 50 kHz, and full-echo acquisition with a half-echo delay of 1.5 ms. For lpMQMAS, both the WURST signal enhancement and the τ_r-pulses were applied with ν_1 = 80 kHz at ν_{irr} = +42ν_r = +588 kHz; a 1 ms WURST-80 pulse was used. The 2D shifted-echo lpMQMAS spectrum was acquired with WURST enhancement, 64 rotor-synchronized t_1 increments, and 96 transients per increment, resulting in a total experiment time of 6 hours. (For interpretation of the references to color in this figure legend, the reader is referred to the web version of this article.)

Now let us turn our attention to a sample that has two inequivalent ^{71}Ga ($S = 3/2$) sites with much larger quadrupolar interactions (β-Ga_2O_3, $C_Q(Ga^{VI})$ = 8.3 MHz and $C_Q(Ga^{IV})$ = 11.2 MHz) [26]. The WURST-enhanced shifted-echo lpMQMAS intensity (Fig. 3a, red trace) of the octahedral site (Ga^{VI}) is ~0.17, while that of the tetrahedral site (Ga^{IV}) is ~0.12, giving an average of 0.15 compared to a spin-echo spectrum. This is remarkable, since to our knowledge MQMAS experiments have not been successfully applied to any half-integer quadrupolar nucleus with ν_Q > 2.5 MHz, even those with relatively high sensitivity, such as ^{11}B, ^{27}Al, ^{71}Ga, ^{87}Rb, etc.; for β-Ga_2O_3, $\nu_Q(Ga^{VI})$ = 4.15 and $\nu_Q(Ga^{IV})$ = 5.6 MHz. Indeed, our attempts at obtaining a high-resolution spectrum using conventional MQMAS pulse sequences was also unsuccessful, yielding only t_1-noise. In fact, prior to our previous work on lpSTMAS [5], a high-resolution ^{71}Ga NMR spectrum of β-Ga_2O_3 was only possible using DAS via specialized hardware [27]. Aside from being able to obtain an lpMQMAS signal for a sample with such large quadrupolar couplings, the similarity in the intensities achieved for two sites (given the relatively large difference in their C_Q values) also serves as validation for the insensitivity of τ_r-pulses and lpMQMAS to the magnitude of quadrupolar interactions.

A ^{71}Ga 2D shifted-echo lpMQMAS NMR spectrum of β-Ga_2O_3 is shown in Fig. 3b. Though there is significant overlap between the ssbs of the two sites in the 1D MAS spectrum due to their large second-order quadrupolar broadening, the two Ga sites are clearly resolved in the 2D spectrum. The t_1 evolution of the spectrum was rotor-synchronized to avoid ssbs in the indirect dimension and improve sensitivity [28], but resulted in aliasing of the signals in f_1 multiple times due to the large spread in frequency of the resonances. For this specific case, the problem can be alleviated via Q-shearing [29] and expansion of the f_1 window to obtain a spectrum where the aliasing is unraveled, as shown in Fig. 3c.

We have chosen examples with $S = 3/2$ nuclei to demonstrate lpMQMAS because the single pair of STs can be treated as isolated two-level systems after placing ν_{irr} far off-resonance with the CT. For $S > 3/2$ nuclei, the presence of other STs introduces further complexity to the theoretical treatment, which gives rise to additional terms in the effective rf Hamiltonian [10,12], and can cause coherence leakage during selective inversion of the inner STs. Further work on lpMQMAS of $S > 3/2$ nuclei is in progress.

5. Practical considerations

The key elements of lpMQMAS experiments are the τ_r-pulses used for selective ST inversion, which allow efficient interconversion of the CT and 3Q coherences. Variation of the τ_r-pulse rf field strength ν_1 shows a well-behaved maximum at ~24 kHz (Fig. 4a). According to the theory, the effective rf field of τ_r-pulses is scaled by the intensity s_n, of the ST spinning sideband nearest to ν_{irr}, which varies among different crystallites. The average intensity assumed for all ST ssbs in Eq. (2) is $|s_n| \sim \sqrt{(\nu_r/1.5\nu_Q)}$, giving a theoretical optimum for lpMQMAS of $\nu_1 \sim \sqrt{(\nu_Q\nu_r/8)}$ = 34 kHz. However, a simulation of the ssbs for one of the STs using an average set of ^{87}Rb quadrupolar parameters (C_Q = 1.9 MHz, η_Q = 0.5) from $RbNO_3$ (Fig. 4b, inset) shows that $|s_n| \approx 0.118$ at ν_{irr} = +220 kHz, approximately twice the ssb intensity s_n^2 compared to the average. After taking this into account, the estimated optimal ν_1 for inversion is approximately $\nu_r/(|s_n|2\sqrt{3})$ = 24.4 kHz, in very good agreement with the experimentally optimized value. In principle, the rf field requirement can be reduced by using longer τ_r-pulses, however, it would increase the effective t_1 evolution due to the longer finite pulse lengths.

The lpMQMAS signal dependence on the τ_r-pulse irradiation frequency ν_{irr} is shown in Fig. 4b for $RbNO_3$. A dramatic enhancement of the efficiency is observed as ν_{irr} moves away from the CT, exhibiting a clear distinction with the on-resonance RIACT method. Since the STs generally spread over hundreds of kilohertz to many megahertz, any ν_{irr} in the range of ±200 to ±500 kHz (depending on the size of C_Q) usually serves as an adequate starting point for calibration, being mindful that the probe tuning bandwidth is usually centered on the CT. Optimization of ν_{irr} should preferably be performed in steps of $n\cdot\nu_r$ to avoid signal modulation due to finite t_1 evolution between the τ_r-pulses. The sign of ν_{irr} has not shown any significant effects experimentally.

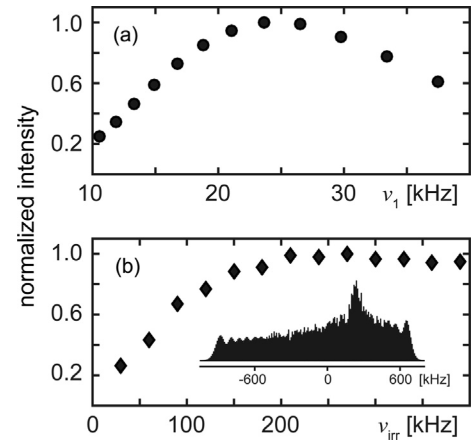

Fig. 4. Shifted-echo lpMQMAS ^{87}Rb NMR signal intensity for the three sites of $RbNO_3$ as a function of the τ_r-pulse (a) rf field ν_1 with ν_{irr} = +220 kHz, and (b) irradiation frequency ν_{irr} with $\nu_1 \approx 24$ kHz. Signal intensities were obtained from integration of spectra in magnitude mode. All other experimental parameters are the same as in Fig. 2. The inset in (b) shows a simulation of the spinning sideband manifold for one the two STs using average ^{87}Rb quadrupolar parameters (C_Q = 1.9-MHz, η_Q = 0.5) for the three sites of $RbNO_3$ [25]. The optimal applied ν_{irr} = +220 kHz is near the peak of the simulated ST ssb manifold.

As stated above, ν_{irr} should be incremented in steps of $n\cdot\nu_r$ during the optimization to avoid the phase modulation due to t_1 evolution. The t_1 evolution delay is defined as the duration between the center of the two τ_r-pulses in Fig. 1c and f. Phase modulation of the signal is observed from changes in ν_{irr}, which may cause confusion during the optimization process. For the phase-modulated shifted-echo lpMQMAS pulse sequence, this problem can be circumvented by displaying spectra in absolute value magnitude mode. However, for amplitude-modulated z-filter sequences, cosine and sine modulated data need to be combined to obtain phase-modulated data. Nonetheless, given that the coherence transfers effected by the τ_r-pulses are identical between the shifted-echo and z-filter sequences, one can simply use the shifted-echo sequence (displayed in absolute value mode) to optimize the τ_r-pulse parameters and avoid the phase modulation observed when changing ν_{irr} over a wide range. Phasing of 2D spectra is not affected, as only an additional zeroth-order phase correction is necessary when the ν_{irr} value is fixed. The rotor-period long pulses applied in lpMQMAS prevent the acquisition of the $t_1 = 0$ increment, which typically helps to determine the direct dimension phasing parameters during 2D spectral processing. This is generally the case for many experiments that employ rotor-synchronized t_1 acquisition, either by preference or necessity, and is not a particular drawback of lpMQMAS experiments. MQMAS spectra are often acquired with rotor-synchronized t_1 evolution such that the aliased ssbs in the indirect f_1 dimension (if any) add up constructively to improve the signal to noise ratio [28]. Given a starting point of $t_1 = \tau_r$, a linear first-order phase correction of the f_1 dimension ($\phi_1 = -360°$) is necessary during spectral processing to compensate for the dwell point missing prior to $t_1 = \tau_r$. Additionally, as t_1 increases, MQMAS time-domain echo signals shift forward with respect to the start of t_2 acquisition by an amount kt_1, where k is the ratio between the second-order quadrupolar broadenings of the 3Q and CT transitions. Therefore, an additional phase correction $\phi_1 = 360° \cdot k\tau_r/(t_2\, dwell)$ needs be applied in the f_2 dimension when experiments are acquired starting at $t_1 = \tau_r$. The ϕ_1 correction in f_2 becomes significant for larger quadrupolar patterns since larger spectral widths (and hence smaller t_2 *dwells*) are required. In this respect, higher MAS frequencies are preferable, both to reduce the ϕ_1 correction necessary in f_2, as well as to obtain larger f_1 spectral widths. In cases where the rotor-synchronized f_1 spectral window is not sufficient to cover the frequency spread of peaks, spectral folding/aliasing can occur, which can be resolved by using *Q*-shearing [29] and subsequent f_1 expansion, as illustrated for β-Ga_2O_3 in Fig. 3.

6. Conclusion

'Low-power' MQMAS methods are introduced which expand the range of quadrupolar interactions for which isotropic spectra can be obtained. The primary source of this capability are 'off-resonance' rotor-period long pulses that can generate triple-quantum coherences from central-transition single-quantum coherences, essentially ST-selective π-pulses. These τ_r-pulses can efficiently manipulate the satellite-transitions and require rf fields which are relatively insensitive to the size of quadrupolar couplings. Thereby allowing acquisition of an isotropic ^{71}Ga NMR spectrum for β-Ga_2O_3, a sample with the largest quadrupolar interactions for which MQMAS spectra has been obtained to date. Additionally, since lpMQMAS experiments rely on CT magnetization, their sensitivity can be enhanced with ST saturation/inversion methods to potentially obtain better signal than conventional MQMAS sequences that use short, high power pulses, as observed for $RbNO_3$. Given the relatively high sensitivity and robustness of lpMQMAS, it can be envisioned as part of heteronuclear NMR experiments to indirectly detect high-resolution correlation spectra of quadrupolar nuclei.

Declaration of Competing Interest

The authors declare that they have no known competing financial interests or personal relationships that could have appeared to influence the work reported in this paper.

Acknowledgements

This work was supported by the National High Magnetic Field Laboratory (NHMFL, USA) through NSF DMR-1644779 and the State of Florida. Use of the NHMFL NMR facility is available free of charge; for more information please visit https://nationalmaglab.org/user-facilities/nmr-mri.

Appendix A

```
; lpmqmasse.ih
; - 2D shifted-echo low-power MQMAS experiment
;ns : 48*n
;p1 : CT soft 90 pulse at PL1
;p7 : ST inversion pulse at SP7
;d0 : initial t1 value
;d1 : recycle delay
;d6 : delay to allow full echo to build up
;in0 : =rotor period for rotor-synchronized
  experiment
;pl1 : CT 90 power level
;sp7 : ST inversion power level
;spnam7 : =square.1000
;spoffs7 : =200-500 kHz
;l6 : number of rotor cycles for D6
;cnst31 : MAS spin rate [Hz]
;FnMODE : QF, F1 REVERSE=TRUE for S=3/2
;zgoptns : -DS3h (for S=3/2), or blank
''p7=1s/cnst31"
''d0=0"
''in0=inf1"
#ifdef S3h
''d6=(1s*l6/cnst31)-(p1*2)"
#else
''d6=(1s*l6/cnst31)-p1"
#endif /* S3h */
1 ze
2 d1
  5u pl1:f1
  (3u ph1):f1
  (p1 ph1 pl1):f1
  (p7:sp7 ph1):f1
  d0
  (p7:sp7 ph2):f1
#ifdef S3h
  (p1*2 ph2 pl1):f1
#endif /* 3h */
  d6
  (p1*2 ph3 pl1):f1
  go=2 ph31
  10m mc #0 to 2 F1QF(id0)
exit
#ifdef S3h
;S=3/2, p=0->-3->+1->-1
ph1=(12) 0 11 10 9 8 7 6 5 4 3 2 1
#else
;S>3/2, p=0->+3->+1->-1
ph1=(12) 0 1 2 3 4 5 6 7 8 9 10 11
#endif /* S3h */
ph2=0
ph3={0}*12 {1}*12 {2}*12 {3}*12
ph31={0 3 2 1 0 3 2 1 0 3 2 1}^2
```

References

[1] A. Samoson, E. Lippmaa, A. Pines, High-resolution solid-state NMR averaging of 2nd-order effects by means of a double-rotor, Mol. Phys. 65 (1988) 1013–1018.
[2] A. Llor, J. Virlet, Towards high-resolution NMR of more nuclei in solids – sample spinning with time-dependent spinner axis angle, Chem. Phys. Lett. 152 (1988) 248–253.
[3] L. Frydman, J.S. Harwood, Isotropic spectra of half-integer quadrupolar spins from bidimensional magic-angle-spinning NMR, J. Am. Chem. Soc. 117 (1995) 5367–5368.
[4] Z. Gan, Isotropic NMR spectra of half-integer quadrupolar nuclei using satellite transitions and magic-angle spinning, J. Am. Chem. Soc. 122 (2000) 3242–3243.
[5] I. Hung, Z. Gan, Low-power STMAS – breaking through the limit of large quadrupolar interactions in high-resolution solid-state NMR spectroscopy, Phys. Chem. Chem. Phys. 22 (2020) 21119–21123, https://doi.org/10.1039/D0CP04274A.
[6] C. Huguenard, F. Taulelle, B. Knott, Z. Gan, Optimizing STMAS, J. Magn. Reson. 156 (2002) 131–137, https://doi.org/10.1006/jmre.2002.2548.
[7] S.E. Ashbrook, S. Wimperis, High-resolution NMR of quadrupolar nuclei in solids: the satellite-transition magic angle spinning (STMAS) experiment, Prog. Nucl. Magn. Reson. Spectrosc. 45 (2004) 53–108.
[8] I. Hung, Z. Gan, High resolution NMR of S = 3/2 quadrupole nuclei by detection of double-quantum satellite-transitions via protons, J. Phys. Chem. Lett. 11 (2020) 4734–4740, https://doi.org/10.1021/acs.jpclett.0c01236.

[9] P. Caravatti, G. Bodenhausen, R.R. Ernst, Selective pulse experiments in high-resolution solid state NMR, J. Magn. Reson. 55 (1983) 88–103, https://doi.org/10.1016/0022-2364(83)90279-2.
[10] A.J. Pell, K.J. Sanders, S. Wegner, G. Pintacuda, C.P. Grey, Low-power broadband solid-state MAS NMR of 14N, J. Chem. Phys. 146 (2017) 194202.
[11] M. Shen, J. Trébosc, O. Lafon, Z. Gan, F. Pourpoint, B. Hu, Q. Chen, J.-P. Amoureux, Solid-state NMR indirect detection of nuclei experiencing large anisotropic interactions using spinning sideband-selective pulses, Solid State Nucl. Magn. Reson. 72 (2015) 104–117, https://doi.org/10.1016/j.ssnmr.2015.09.003.
[12] I. Hung, P. Gor'kov, Z. Gan, Efficient and sideband-free 1H-detected 14N magic-angle spinning NMR, J. Chem. Phys. 151 (2019), https://doi.org/10.1063/1.5126599 154202.
[13] J.P. Amoureux, C. Fernandez, S. Steuernagel, Z filtering in MQMAS NMR, J. Magn. Reson. A. 123 (1996) 116–118.
[14] J.-P. Amoureux, C. Fernandez, L. Frydman, Optimized multiple-quantum magic-angle spinning NMR experiments on half-integer quadrupoles, Chem. Phys. Lett. 259 (1996) 347–355, https://doi.org/10.1016/0009-2614(96)00809-3.
[15] H.T. Kwak, Z.H. Gan, Double-quantum filtered STMAS, J. Magn. Reson. 164 (2003) 369–372.
[16] D. Massiot, B. Touzo, D. Trumeau, J.P. Coutures, J. Virlet, P. Florian, P.J. Grandinetti, Two-dimensional magic-angle spinning isotropic reconstruction sequences for quadrupolar nuclei, Solid State Nucl. Magn. Reson. 6 (1996) 73–83.
[17] S.P. Brown, S. Wimperis, Two-dimensional multiple-quantum MAS NMR of quadrupolar nuclei: A comparison of methods, J. Magn. Reson. 128 (1997) 42–61.
[18] G. Wu, D. Rovnyak, R.G. Griffin, Quantitative multiple-quantum magic-angle-spinning NMR spectroscopy of quadrupolar nuclei in solids, J. Am. Chem. Soc. 118 (1996) 9326–9332.
[19] Z. Yao, H.T. Kwak, D. Sakellariou, L. Emsley, P.J. Grandinetti, Sensitivity enhancement of the central transition NMR signal of quadrupolar nuclei under magic-angle spinning, Chem. Phys. Lett. 327 (2000) 85–90, https://doi.org/10.1016/S0009-2614(00)00805-8.
[20] D. Iuga, A.P.M. Kentgens, Influencing the satellite transitions of half-integer quadrupolar nuclei for the enhancement of magic angle spinning spectra, J. Magn. Reson. 158 (2002) 65–72, https://doi.org/10.1016/S1090-7807(02)00061-7.
[21] R. Siegel, T.T. Nakashima, R.E. Wasylishen, Signal enhancement of NMR spectra of half-integer quadrupolar nuclei in solids using hyperbolic secant pulses, Chem. Phys. Lett. 388 (2004) 441–445.
[22] Q. Wang, J. Trebosc, Y. Li, O. Lafon, S. Xin, J. Xu, B. Hu, N. Feng, J.-P. Amoureux, F. Deng, Uniform signal enhancement in MAS NMR of half-integer quadrupolar nuclei using quadruple-frequency sweeps, J. Magn. Reson. 293 (2018) 92–103, https://doi.org/10.1016/j.jmr.2018.06.005.
[23] E. Kupce, R. Freeman, Adiabatic pulses for wide-band inversion and broad-band decoupling, J. Magn. Reson. A. 115 (1995) 273–276.
[24] K.K. Dey, S. Prasad, J.T. Ash, M. Deschamps, P.J. Grandinetti, Spectral editing in, solid-state MAS NMR of quadrupolar nuclei using selective satellite inversion, J. Magn. Reson. 185 (2007) 326–330.
[25] J. Skibsted, H.J. Jakobsen, Variable-temperature Rb-87 magic-angle spinning NMR spectroscopy of inorganic rubidium salts, J. Phys. Chem. A. 103 (1999) 7958–7971.
[26] T. Vosegaard, I.P. Byriel, L. Binet, D. Massiot, H.J. Jakobsen, Crystal structure studies by single-crystal NMR spectroscopy. Ga-71 and Ga-69 single-crystal NMR of beta-Ga2O3 twins, J. Am. Chem. Soc. 120 (1998) 8184–8188.
[27] D. Massiot, I. Farnan, N. Gautier, D. Trumeau, P. Florian, P. Grandinetti, 69Ga,71Ga solid-state static, MAS and DAS NMR-study of beta-Ga2O3, J. Chim. Phys.-Chim. Biol. 92 (1995) 1847–1850, https://doi.org/10.1051/jcp/1995921847.
[28] D. Massiot, Sensitivity and lineshape improvements of MQ-MAS by rotor-synchronized data acquisition, J. Magn. Reson. A. 122 (1996) 240–244.
[29] I. Hung, J. Trebosc, G.L. Hoatson, R.L. Vold, J.P. Amoureux, Z. Gan, Q-shear transformation for MQMAS and STMAS NMR spectra, J. Magn. Reson. 201 (2009) 81–86.